

# Gated transport in nanofluidic devices

Xiaozhong Jin · N. R. Aluru

Received: 23 December 2010 / Accepted: 18 March 2011 / Published online: 10 April 2011  
© Springer-Verlag 2011

**Abstract** The surface property of the nanochannel plays an important role in controlling the ion transport through the nanochannel. Embedding electrodes outside the nanochannel (referred to as gated nanochannels) is a simple way to control the surface charge density of the nanochannel. Based on the numerical simulations using coupled Poisson–Nernst–Planck and Stokes equations, we show that a relative difference between the applied voltage and the gate voltage would alter the space charge density along the nanochannel. Thus, the gate voltage can tune the nanochannel into a *p*- or *n*-type field effect transistor, enabling the control of fluid flow in the nanochannel. The ionic currents reveal that the ionic flux can be controlled by the gate voltage. Analytical expressions are derived to estimate the effective space charge density and the fluid flow in the nanochannels for a fixed gate voltage. We also suggest potential applications of the gated nanochannels.

**Keywords** Nanofluidic · Gate · Space charge · Diodes · Preconcentration

## 1 Introduction

With advances in fabrication techniques, some unique features of nanofluidics, such as permselectivity, localized

space charges, concentration polarization, etc., have led to novel applications in lab-on-a-chip analyses. Modulated ion transport plays a significant role in biological sensing, sample separation, mixing, and drug delivery (Hong and Quake 2003; Yao et al. 2006; Reyes et al. 2002; Auroux et al. 2002). Integrating functional nanoscale components with microfluidic devices has led to promising ways of manipulating individual molecules (Yaroshchuk et al. 2005; Eijkel and van den Berg 2005; de Jong et al. 2006; Jeon et al. 2005; Wang et al. 2005; Fan et al. 2005; Pu et al. 2004; Kuo et al. 2003a, 2003b; Tulock et al. 2004; Kuo et al. 2004; Chatterjee et al. 2005; Gatimu et al. 2006; Gatimu et al. 2008). In nanofluidic systems, ion transport, as well as the fluid flow, can be regulated by the surface charge on the nanochannel, especially when the Debye length is comparable to the nanochannel width (Schoch et al. 2005; Schoch and Renaud 2005; Stein et al. 2004). A typical example is a nanofluidic diode, where a cation-exchange nanopore (negative surface charge) in conjunction with an anion-exchange nanopore (positive surface charge) creates an asymmetric surface charge distribution along the nanochannel and results in an ionic current rectification (Daiguji et al. 2005; Karnik et al. 2007; Vlassiouk and Siwy 2007; Kalman et al. 2008). The development of new techniques to effectively tune the surface charge is an area of immense interest that can have a profound impact on nanofluidic applications.

Several developments have been reported to modulate the surface charge on the wall (Horvath and Dolnik 2001; Belder and Ludwig 2003; Long et al. 2006; Prakash et al. 2007, 2009), including the manipulation of buffer concentrations, addition of surfactants and surface-active materials to analyte solutions, and manipulating the solution pH. The basic idea in these methods is to control the interaction between the solution in the channel and the

X. Jin · N. R. Aluru (✉)  
Department of Mechanical Science and Engineering, Beckman  
Institute for Advanced Science and Technology,  
University of Illinois at Urbana-Champaign,  
Urbana, IL 61801, USA  
e-mail: aluru@illinois.edu  
URL: <http://www.illinois.edu/~aluru>

double layer at the channel wall surface. Surface coating via physically or chemically adding functional groups to the wall has received significant interest. Techniques such as, diffusion-limited patterning, have been used to dope avidin onto the surface to generate a discontinuous surface charge distribution in a nanochannel (Karnik et al. 2007). Silicon-based nanochannels enable embedding gate electrodes outside the nanochannel to tune the surface charge, which provides a simple and a fast electrostatic control scheme. Various applications based on the adjustment of the local surface charge on the microchannels have demonstrated successful control of the electroosmotic flow in microchannels (Schasfoort et al. 1999; Horiuchi and Dutta 2006; Lin et al. 2006). In nanochannels, embedding electrodes can not only control the electroosmotic flow, but also affect ion concentrations in the system. Recent experiments have indicated that conductance in the nanochannel can be controlled by applying an external voltage on the gate (Schoch and Renaud 2005). With gate modulation, the ionic current exhibits a nonlinear increase with the applied electric potential, which is similar to that of the current-voltage relations observed in some semiconductor devices. Owing to the fast ion transport, gated nanochannels have potential applications as electrochemical energy conversion devices (Vermesh et al. 2009; Fan et al. 2008; Moghaddam et al. 2010).

Although significant progress has been made in fabricating and designing gated nanofluidic devices, the underlying transport physics is not fully understood, e.g., the effect of the gate voltage on the surface charge density in the gated nanochannel. Modeling and simulation can provide immense details in explaining the underlying physical mechanisms observed in the experiments and in enhancing the capabilities of gated nanofluidic devices. The continuum theory has been shown to successfully predict the ion transport and some other properties of nanofluidic channels (Daiguji et al. 2004; Jin et al. 2007). Most continuum models describe the ionic transport by the Poisson and the Nernst–Planck equations (PNP). A review of the theory and simulations on fundamental studies in nanochannels is given in (Baldessari and Santiago 2006; Pennathur and Santiago 2005; Karniadakis et al. 2005). In this article we perform extensive numerical studies based on the continuum theory to understand the effect of gate voltage on the surface charge density, fluid flow and ion transport. We also develop analytical theories to predict most of the characteristics of gated nanofluidic devices. The simulation studies also suggest potential applications of gated nanofluidic devices as diodes and preconcentration devices. The rest of this article is outlined as follows: Sect. 2 presents the theory and the mathematical model, Sect. 3 describes the canonical micro-nanofluidic device on which gated transport studies are performed, Sect. 4 presents the

simulation results and discussion, and conclusions are given in Sect. 5.

## 2 Theory

In this section, a description of the complete set of equations that are used for simulation of electrokinetic transport in hybrid micro-nanofluidic channels is presented. When the flow is electrically driven, the total flux consists of three terms: a diffusive component resulting from the concentration gradient, an electrophoretic component, which stems from the electrical potential gradient, and a convective component which originates from the fluid flow. The total flux of the  $i$ th species is given by the expression

$$\Gamma_i = -D_i \nabla c_i - \Omega_i z_i F c_i \nabla \phi + c_i \mathbf{u} \quad (1)$$

where  $F$  is Faraday's constant,  $z_i$  is the valence,  $D_i$  is the diffusion coefficient,  $\Omega_i$  is the ionic mobility,  $\Gamma_i$  is the flux vector,  $c_i$  is the concentration of the  $i$ th species,  $\mathbf{u}$  is the velocity vector of the bulk flow, and  $\phi$  is the electrical potential. The three terms on the right-hand side of Eq. 1 define the fluxes because of diffusion, electrical migration, and convection, respectively. The electrical potential distribution is governed by the Poisson equation

$$\nabla \cdot (\epsilon_r \nabla \phi) = -\frac{\rho_s}{\epsilon_0} \quad (2)$$

where  $\epsilon_0$  is the permittivity of vacuum,  $\epsilon_r$  is the relative permittivity, and  $\rho_s$  is the space charge density. The space charge density is defined by

$$\rho_s = F \sum_{i=1}^m z_i c_i \quad (3)$$

where  $m$  is the total number of species in the system.  $\epsilon_r = 80$  is used in the solution, and  $\epsilon_r = 4$  is used in the oxide layer.

The material-balance equation or the Nernst–Planck (NP) equation describes the mass transfer of each dissolved species and is given by

$$\frac{\partial c_i}{\partial t} = -\nabla \cdot \Gamma_i \quad (4)$$

In micro and nanometer channels, the Reynolds number is low and the convective term in the Navier–Stokes equation can be neglected. Therefore, the Stokes equation and continuity equation are solved to obtain the velocity distribution. The Stokes equation for the velocity and the continuity equation for the incompressible fluid describe the movement of the fluid through the channels and are given by

$$-\nabla p + \mu \nabla^2 \mathbf{u} - \rho_s \nabla \phi = 0 \quad (5)$$

$$\nabla \cdot \mathbf{u} = 0 \quad (6)$$

In the above equations,  $p$  is the hydrostatic pressure, and  $\mu$  is the fluid viscosity. The third term in Eq. 5 is the body force acting on the fluid due to the space charges and the electric field.

The coupled Poisson–Nernst–Planck equations (PNP) and the Stokes equations are solved using the finite cloud method (Aluru 2000; Aluru and Li 2001; Jin et al. 2001; Jin et al. 2004; Jin et al. 2005). The computed solutions include the electric potential, ionic concentration, velocity, and pressure profiles in the system. The current through the channel is calculated by integrating the ionic fluxes over the cross-section, i.e.,

$$\mathbf{I} = \int_S \sum_i z_i F \Gamma_i dS \quad (7)$$

where  $S$  is the cross-sectional area of the channel. Note that the depth (the third dimension) is taken as 1 m in this article.

### 3 Simulation setup

In this study, we consider a canonical problem as shown in Fig. 1. The bath connected to electrode 1 is designated as reservoir 1 and the bath connected to electrode 2 is designated as reservoir 2.  $V_D$  is the voltage applied on electrode 1, and electrode 2 is grounded.  $V_G$  is the voltage applied on the oxide layer. Note that the electrode deposited on the oxide layer could be an array such that the applied gate voltage is not necessarily a constant along the nanochannel. Both reservoirs are identical in size and have a length of 1  $\mu\text{m}$  and a width of 1  $\mu\text{m}$ . The nanochannel is 2  $\mu\text{m}$  long and 10 nm wide. The thickness of the oxide layer is 300 nm. The currents are measured at electrode 1 and electrode 2.

We perform two-dimensional simulations by assuming that the depth of the micro and nanochannels is much larger

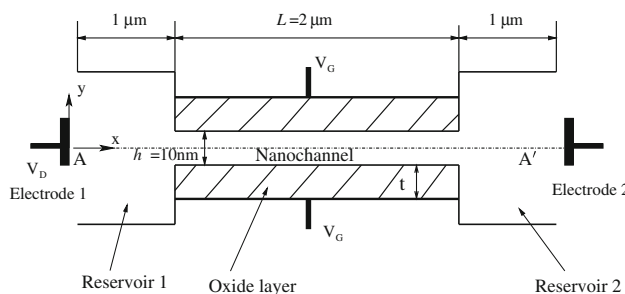


**Fig. 1** A canonical micro-nanofluidic system not drawn to scale. Note the position of the origin of the coordinate system and the placement of the  $x$ - and  $y$ -axes

than the width. The baths are filled with 1 mM KCl solution. The diffusivities of  $\text{K}^+$  and  $\text{Cl}^-$  are taken to be  $1.96 \times 10^{-9} \text{ m}^2/\text{s}$  and  $2.03 \times 10^{-9} \text{ m}^2/\text{s}$ , respectively. The boundary conditions for ionic concentrations at the ends of the baths are given by a constant value of 1 mM. The normal flux of each ion is assumed to be zero on all the channel walls. The ion concentrations in the oxide layer are assumed to be zero. At the interface, which separates the nanochannel and the oxide layer, electric field is not continuous due to the discontinuity of electric permittivities and surface charges on the nanochannel wall. The electric potential at the interface is governed by the Gauss's Law (Jackson 1999)

$$\epsilon_{ox} \frac{\partial \phi}{\partial n}|_{ox} + \epsilon_w \frac{\partial \phi}{\partial n}|_w = -\frac{\sigma_f}{\epsilon_0} \quad (8)$$

where  $\epsilon_{ox}$  is the dielectric constant of the oxide layer,  $\epsilon_w$  is the dielectric constant of the solution,  $\frac{\partial \phi}{\partial n}|_{ox}$  is the normal derivative of the electric potential pointing toward the oxide layer,  $\frac{\partial \phi}{\partial n}|_w$  is the normal derivative of the electric potential pointing toward the nanochannel, and  $\sigma_f$  is the fixed surface charge density of the nanochannel wall. Normally, lower surface charge densities require a smaller gate voltage to effect a polarity change in the nanochannel. Majumdar's group reduced the magnitude of the surface charge density to less than 0.2 mC/m<sup>2</sup> by modifying the native silica surface, and successfully manipulated protein transport using 1 Volt gate voltage (Karnik et al. 2006). In the simulation, we use  $-0.2 \text{ mC/m}^2$  as the surface charge density of the nanochannel. At low gate voltages (in the range of a few Volts), it is assumed that the gate voltage has little or no effect on SiOH dissociation of the wall, so that the fixed surface charge density is not varying with the gate voltage.

Nonslip boundary conditions are assumed on the channel walls for the fluid velocities. Pressure is assumed to be zero at the ends of reservoirs 1 and 2. The pressure boundary conditions on the walls are corrected by enforcing continuity, Eq. 6, on the walls.

### 4 Results and discussion

In this section, we investigate how the applied gate voltage changes the space charges in the nanochannel. For a fixed surface charge density and an applied gate voltage, we derive an analytical expression for the induced space charges in the nanochannel. The induced space charges under an external electric field give rise to the fluid flow in the nanochannel. An analytical solution is derived for the velocity profile in the nanochannel to show the relationship between the fluid flow and the applied potentials. We also investigate the variation of ionic current with the applied

potential. An analytical solution is derived for the ionic current to explain the effect of the gate voltage. Furthermore, with asymmetric gate voltages we show that it is possible to obtain rectification and preconcentration.

#### 4.1 Space charges in the nanochannel

Surface charge plays a crucial role in controlling the ion transport in the nanochannel. In the presence of gate electrode, the effective surface charge on the nanochannel wall is a combination of the fixed surface charge (due to the functional groups on the surface) and the induced surface charge due to the applied gate voltage. In this study, we ignore the water dissociation in the nanochannel since the ion concentration in the nanochannel is much larger than the  $H^+$  and  $OH^-$  concentration. Theoretically, the induced surface charge is directly related to the electric field from the applied gate voltage. Since the resistance in the nanochannel is much larger than that in the reservoirs for low applied voltages, the electric potential drop mainly occurs in the nanochannel. Figure 2a shows the electric potential profile along the central line of the system. Note that the nanochannel starts at  $x = 1 \mu m$  and ends at  $x = 3 \mu m$ . Although the applied gate potential changes the potential profile, it is assumed that the electric potential drops linearly in the nanochannel in deriving an analytical equation for the space charge density.

Integrating Eq. 2 over a small control volume across the nanochannel and using the divergence theorem, we obtain

$$\oint_{\Delta S} \epsilon_r \nabla \phi \cdot \mathbf{n} dS = - \iint_{\Delta V} \frac{\rho_s}{\epsilon_0} dV \quad (9)$$

where  $\Delta S$  is the surface of the control volume,  $\mathbf{n}$  is the normal direction of the surface, and  $\Delta V$  is the volume. Applying Gauss's Law at the wall and considering linear potential drop along the  $x$ -direction, we obtain

$$-2\epsilon_{ox}E_{ox} = \frac{2\sigma_f}{\epsilon_0} + \frac{\rho_e h}{\epsilon_0} \quad (10)$$

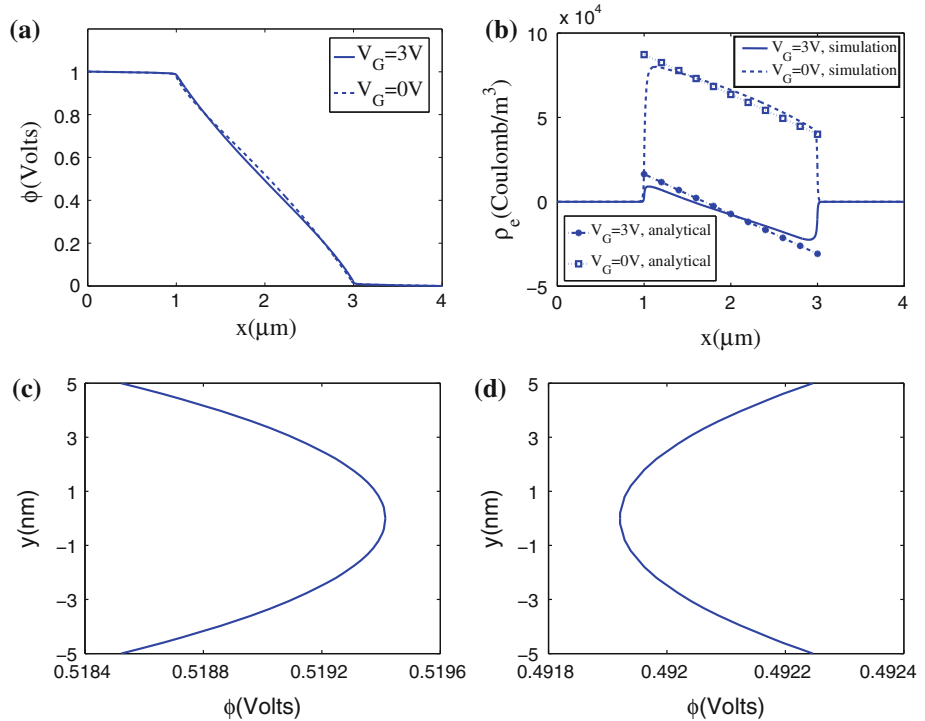
where  $\epsilon_{ox}$  is the dielectric constant of the oxide layer.  $\sigma_f$  is the fixed surface charge density on the nanochannel wall.  $\rho_e$  is the averaged space charge density across the nanochannel, i.e.,

$$\rho_e = \frac{1}{h} \int_{-\frac{h}{2}}^{\frac{h}{2}} \rho_s dy \quad (11)$$

$E_{ox}$  is the electric field in the  $y$ -direction on the channel wall directed toward the oxide layer side. Since the aspect ratio of the oxide layer length to its thickness is high, the electric field in the oxide layer can be approximated as

$$E_{ox} = \frac{V_G - \phi}{t} \quad (12)$$

**Fig. 2** **a** Electric potential profile along the central line AA' when  $V_D = 1V$ . **b** Averaged space charge density along the channel with various gate voltages when  $V_D = 2V$ . The analytical solutions are calculated using Eq. 14. **c** Electric potential across the nanochannel at  $x = 2 \mu m$ , when  $V_D = 1V$  and  $V_G = 0V$ . **d** Electric potential across the nanochannel at  $x = 2 \mu m$ , when  $V_D = 1V$  and  $V_G = 3V$



where  $t$  is the thickness of the oxide layer.  $\phi$  is the potential at the wall of the nanochannel. Hence, the electric field in the oxide layer can be estimated by

$$E_{\text{ox}} = \frac{1}{t} \left[ V_G - V_D \left( 1 - \frac{x - x_s}{L} \right) \right] \quad (13)$$

where  $L$  is the length of the nanochannel, and  $x_s$  is the  $x$  coordinate where the nanochannel starts. Hence, the cross-sectional averaged space charge density in the nanochannel ( $x_s \leq x \leq x_s + L$ ) can be estimated as

$$\rho_e = -\frac{2\sigma_f}{h} - \frac{2\epsilon_{\text{ox}}\epsilon_0}{ht} \left( V_G - V_D \left( 1 - \frac{x - x_s}{L} \right) \right) \quad (14)$$

The first term on the right hand side of Eq. 14 is caused by the fixed charge density on the nanochannel, while the second term is induced by the gate voltage. With an applied gate voltage, the resulting space charge density in the nanochannel is a function of the applied gate voltage and varies linearly along the nanochannel. Once the space charge densities are known, the effective surface charge density of the nanochannel can be calculated from the electroneutrality condition (Daiguji et al. 2004; Vermesh et al. 2009)

$$\sigma_e = -\frac{\rho_e h}{2} \quad (15)$$

Figure 2b shows the averaged space charge density along the channel when  $V_D$  is 2V. For the numerical simulation value, the space charge density is averaged by integrating along the  $y$ -direction and normalized by the width. We observe that the space charge density decreases linearly along the nanochannel. For  $V_G = 3V$ , bi-polarity is observed in the nanochannel (left part of the nanochannel is positively charged while the right part of the channel is negatively charged). This result indicates that one can easily control the polarity of the nanochannel during the operation by changing the gate voltage, which also can be justified by the electric potential across the nanochannel. Figure 2c and d shows the electric potential profiles across the nanochannel at  $x = 2 \mu\text{m}$  for different gate voltages. When  $V_G = 0V$ , since the space charges in the nanochannel are positive corresponding to a negative effective surface charge, the electric potential at the wall ( $y = 5 \text{ nm}$ ) is lower than that at the center ( $y = 0 \text{ nm}$ ), as shown in Fig. 2c. However, as the gate voltage increases to  $V_G = 3V$ , the gate voltage makes the effective surface charge positive, so that the electric potential at the wall ( $y = 5 \text{ nm}$ ) is higher than that at the center ( $y = 0 \text{ nm}$ ), as shown in Fig. 2d. The calculated (analytical) space charge densities in the nanochannel, using Eq. 14, are also plotted in Fig. 2b, which match reasonably well with the simulation results. Equation 14 indicates that the space charge in the nanochannel also depends on the thickness of the oxide

layer. The thinner the oxide layer, the stronger is its effect on the space charge density due to the gate voltage.

#### 4.2 Electroosmotic flow

It is well-known that electroosmotic flow depends on the zeta-potential and on the applied external electric field. As the gate voltage can change the zeta-potential on the surface, Lee et al. has shown for microchannels the relationship between the applied control voltage and the electroosmotic flow (Lin et al. 2006). Similar to the microchannel case, the applied gate voltage can also control the fluid flow in the nanochannel. But the velocity profiles derived for the microchannel case may not be valid in the nanochannel case due to the overlap of the electric double layers. We can estimate the velocity profile in the nanochannel once we know the effective surface charge density (or the induced space charges in the nanochannel). Using the Stokes equation, we can derive the velocity in the nanochannel as follows:

$$\int_{-\frac{h}{2}}^{\frac{h}{2}} \int_{x_s}^{x_s+L} \mu \nabla^2 u dx dy = \int_{-\frac{h}{2}}^{\frac{h}{2}} \int_{x_s}^{x_s+L} \left( \frac{\partial p}{\partial x} + \rho_s \frac{\partial \phi}{\partial x} \right) dx dy \quad (16)$$

where the left hand side can be evaluated by using the divergence theorem.

$$\int_{-\frac{h}{2}}^{\frac{h}{2}} \int_{x_s}^{x_s+L} \mu \nabla^2 u dx dy = \oint_S \mu \nabla u \cdot \mathbf{n} dS \quad (17)$$

Invoking several assumptions such as (1) the pressure at both ends of the nanochannel is the same (the baths are open to the atmosphere), (2) the electric field is constant along the nanochannel, (3) the fluid flow in the nanochannel is well developed, (4) the velocity profile across the nanochannel is parabolic (due to the overlapped double layers in the nanochannel), and (5) the applied potential drops linearly along the nanochannel, Eq. 16 can be simplified as

$$2 \mu \frac{\partial u}{\partial y} \Big|_{y=h/2} L = -\frac{V_D}{L} \int_{x_s}^{x_s+L} \rho_e dx dy \quad (18)$$

It means that the viscous force from the nanochannel wall should equal the body force due to the space charges and the axial electric field. The  $x$ -component of the velocity across the nanochannel is assumed as

$$u = u_c \left[ 1 - \left( \frac{y}{h/2} \right)^2 \right] \quad (19)$$

where  $u_c$  is the  $x$ -component of velocity at the center of the nanochannel. Substituting the approximation for space charge (given in Eq. 14) in Eq. 18, we obtain

$$u_c = -\frac{V_D h}{4 \mu L} \left( \sigma_f + \frac{\epsilon_{ox} \epsilon_0}{t} (V_G - 0.5 V_D) \right) \quad (20)$$

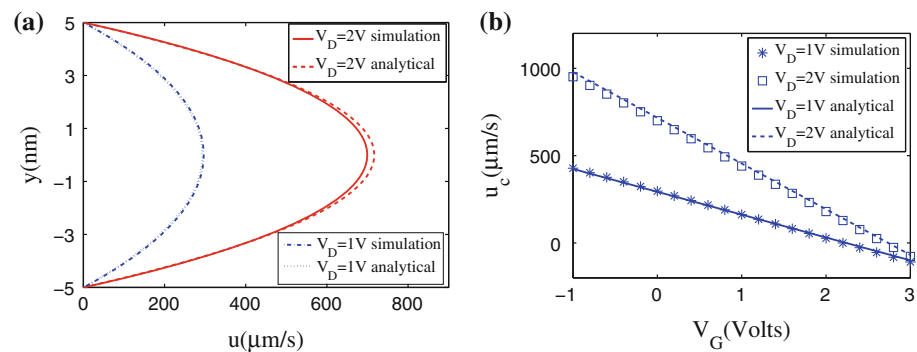
As the pressure loss in the bath and at the entrance/exit of the nanochannel are neglected, the velocity in the nanochannel is expected to be lower than that calculated from Eq. 20. Therefore, we use the following equation to estimate the fluid velocity in the nanochannel:

$$u_c = -\frac{0.92 V_D h}{4 \mu L} \left( \sigma_f + \frac{\epsilon_{ox} \epsilon_0}{t} (V_G - 0.5 V_D) \right) \quad (21)$$

where the correction factor 0.92 is obtained by fitting with the simulation data. Fig. 3a shows the velocity profiles across the nanochannel when the gate voltage is 0 V. Note that the velocity profile obtained from simulations across the nanochannel is parabolic. The velocities calculated from Eq. 21 match well with the simulation results. The maximum velocity in the nanochannel as a function of the gate voltage is plotted in Fig. 3b. In this case, the fixed surface charge density is assumed to be  $-0.2 \text{ mC/m}^2$ . When the gate voltage is smaller than the applied voltage  $V_D$ , the space charge density is positive. The velocity is positive, which implies that the fluid flow is from left to right. As the gate voltage increases, the absolute value of the space charge reduces, resulting in a lower velocity. When the gate voltage increases to a value such that the polarity in the nanochannel becomes negative, the fluid velocity becomes negative, indicating the direction of the fluid flow has reversed. Both the simulation and analytical solution show that the velocity is a linear function of the gate voltage.

Figure 3b indicates that the fluid flow in the nanochannel can be easily controlled by varying the gate voltage. It is important to note that the gate voltage is not necessarily a constant along the nanochannel. As in the microchannel case, with different voltages applied on the top and bottom oxide layer, one can generate more complicated fluid flows to enhance the mixing of species.

**Fig. 3** **a** The  $x$ -component of velocity across the nanochannel when  $V_G = 0 \text{ V}$ . The analytical solutions are calculated from Eq. 21. **b** Variation of the maximum velocity (which is at the central line),  $u_c$  in the  $x$ -direction, in the nanochannel as a function of  $V_G$ .



#### 4.3 Ionic current

The ionic current depends on several variables including the ion concentrations and the external electric field. In microchannels, the double layer is very thin compared to the channel width. As a result, the ionic concentration outside the double layer, which is a significant portion of the microchannel, is equal to the bulk value and the gate voltage has minor effect on the ion concentrations and the electric field along the microchannel. However, in the case of the nanochannel, the double layers can overlap and the ionic concentrations in the channel can depend on the applied gate voltage. Hence, the gate voltage applied on the nanochannel can control the ion transport in the nanochannel. To further understand the effect of the gate voltage, we compute the I-V (current versus voltage) curves as a function of the applied gate voltage. The relationship between the ionic current and the applied voltage can be understood by looking at the one-dimensional form of Eqs. 1 and 4. We will assume that the diffusion coefficients of the cations and the anions are identical and denote it as  $D$ . Ignoring the diffusion and convection terms in Eq. 1, the current in the  $x$ -direction can be estimated by

$$I_x = -\frac{D z^2 F^2}{RT} \frac{\partial \phi}{\partial x} \int_{-\frac{h}{2}}^{\frac{h}{2}} (c_1 + c_2) dx \quad (22)$$

Assuming the electric potential drops linearly along the  $x$ -direction, we obtain

$$I_x = \frac{D z^2 F^2 V_D}{RT L^2} \int_{x_s}^{x_e} (\bar{c}_1 + \bar{c}_2) dx \quad (23)$$

where  $\bar{c}_1$  and  $\bar{c}_2$  are the averaged concentrations of the cations and anions along the  $y$ -direction, respectively,  $x_s$  is the coordinate where the nanochannel starts,  $x_e$  is the coordinate where the nanochannel ends, and  $z$  is the valence of ions. The ion concentration can be estimated by (Schoch and Renaud 2005)

$$\bar{c}_1 + \bar{c}_2 = 2c_0 + \frac{|\rho_e|}{F} \quad (24)$$

where  $c_0$  is the bulk concentration in the bath. Hence, the current can be calculated by

$$I_x = I_0 \left[ 1 + \frac{|\rho_e|}{2c_0 F} \right] \quad (25)$$

where  $I_0$  is the current when there is no space charge in the nanochannel and is given by

$$I_0 = \frac{2Dz^2 F^2}{RT} c_0 V_D / L \quad (26)$$

and  $|\rho_e|$  is the absolute value of the space charge density averaged in the nanochannel,

$$|\rho_e| = \frac{1}{L} \int_{x_s}^{x_e} |\rho_e| dx \quad (27)$$

where  $\rho_e$  is calculated from Eq. 14.

Figure 4a shows the space charge density at the center of the nanochannel. Figure 4b shows the I-V curves when the gate voltage changes from -1 to 3 V. In all these cases, the fixed surface charge density is  $-0.2\text{mC/m}^2$  in the nanochannel. We observe that when the gate voltage increases, the current decreases until a certain gate voltage and increases again with a further increase in the gate voltage. As the gate voltage increases from -1 V, the space charge density in the nanochannel decreases, which reduces the conductance in the nanochannel. With a further increase in the gate voltage, the space charge density becomes negative, and the absolute value of the space charge density increases resulting in an increase in the conductance in the nanochannel. The ionic current calculated from Eq. 25, which relates the ionic current to the space charge density, matches reasonably well with the numerical simulation results when  $V_D$  is 0.5 V. However, for a higher  $V_D$ , the ionic current from the numerical simulation is higher than that calculated from Eq. 25. This implies that a higher  $V_D$  magnifies the impact of the

effective surface charge on the ion transport. Note that the ionic current when  $V_D$  is 1 V is more than twice the ionic current when  $V_D$  is 0.5 V, indicating an enhancement of the ion transport.

#### 4.4 Nanofluidic diode

The functionality of the nanochannel can be tuned into a diode, akin to the solid-state diode, by controlling the space charge density in the nanochannel. By applying a certain pattern of gate voltage on the nanochannel, one can control the polarity of the nanochannel to obtain an asymmetric charge density in the nanochannel. For example, on the left half of the nanochannel (from  $x = 1.0\text{\mu m}$  to  $x = 2.0\text{\mu m}$ ) a positive gate voltage can be applied (applied gate voltage is  $V_G$ ), and on the right half (from  $x = 2.0\text{\mu m}$  to  $x = 3.0\text{\mu m}$ ) a negative gate voltage can be applied (applied gate voltage is  $-V_G$ ). When  $V_D$  is negative, the cation migrates from the right reservoir to the left reservoir and is favored to get into the nanochannel due to the *n*-type polarity in the right part of the nanochannel, and the anion migrates from the left reservoir to the right reservoir and is favored to get into the nanochannel due to the *p*-type polarity in the left part of the nanochannel. Cations and anions accumulate in the nanochannel, resulting in high conductance in the nanochannel. However, with a positive applied potential  $V_D$ , the migration direction of the cation and anion is reversed. The polarity in the left part of the nanochannel restricts the cations from getting into the nanochannel, and the polarity in the right part of the nanochannel restricts the anions from getting into the nanochannel. The unfavorable polarization results in a low conductance in the nanochannel. Figure 5a shows the ionic current as a function of the drain voltage for different  $V_G$ . As expected, the ionic current when a negative  $V_D$  is applied is much higher compared to the current when a positive  $V_D$  is applied. As  $V_G$  increases, the ionic current increases when  $V_D$  is negative, and decreases when  $V_D$  is positive. The rectification factor as a function of  $V_G$  is shown in Fig. 5b. The rectification factor is defined as the

**Fig. 4** a The effect of gate voltage on the space charge density at the center of the nanochannel ( $x = 2\text{\mu m}$ ). b The ionic current measured at the end of reservoir 1 as a function of the gate voltage

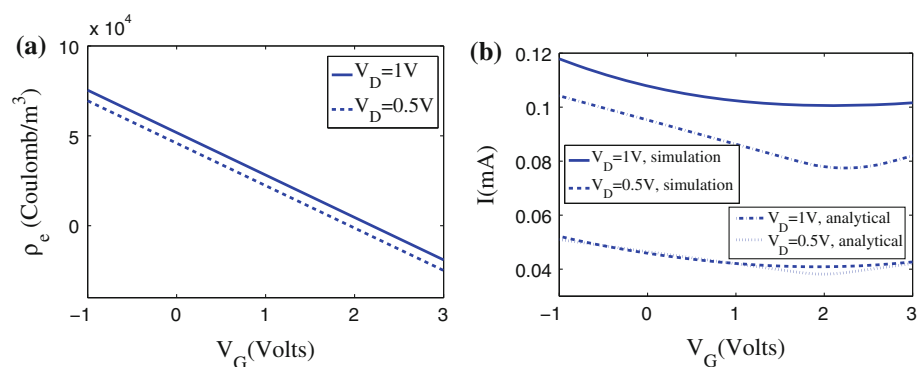


**Fig. 5** Nanofluidic diodes. **a** The ionic current with the drain voltage under various gate voltages. **b** The rectification factor with the gate voltage

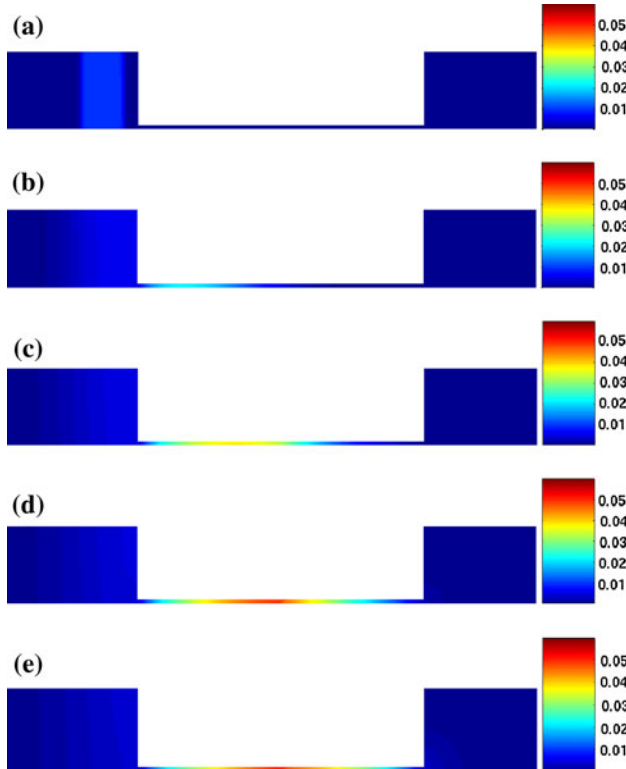
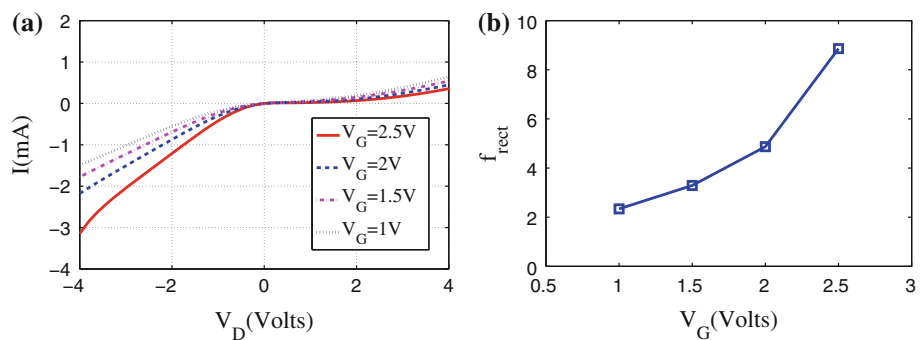


**Fig. 6**  $\text{Rd}^+$  concentrations at different times. **a**  $t = 0$ . **b**  $t = 10 \mu\text{s}$ . **c**  $t = 20 \mu\text{s}$ . **d**  $t = 30 \mu\text{s}$ . **e**  $t = 40 \mu\text{s}$ . Note that only half of the system is plotted due to the symmetry

ratio of the ionic current when  $V_D = -4 \text{ V}$  to the ionic current when  $V_D = 4 \text{ V}$ . The higher, the  $V_G$ , the higher is the polarity difference in the nanochannel resulting in a higher induced charge gradient, and hence, a higher rectification factor. We observe that the rectification factor increases nonlinearly with the gate voltage.

#### 4.5 Preconcentration

As another example, in this section, we demonstrate sampling and concentrating dilute species by manipulating the applied potentials. Initially, there is a plug of  $\text{Rd}^+$  in the left bath (starting from  $x = 0.5 \mu\text{m}$  to  $x = 0.8 \mu\text{m}$ ), as shown in Fig. 6a. The initial concentration of  $\text{Rd}^+$  is

0.01 mM. We can transport the species into the nanochannel by setting  $V_D$  to 1 V. We also apply  $-2 \text{ V}$  gate voltage on the left half of the nanochannel (from  $x = 1.0 \mu\text{m}$  to  $x = 2.0 \mu\text{m}$ ), and 2 V gate voltage on the right half of the nanochannel (from  $x = 2.0 \mu\text{m}$  to  $x = 3.0 \mu\text{m}$ ). Because the electric potential is higher in the left bath compared to that in the right bath,  $\text{Rd}^+$  moves from the left reservoir to the right reservoir. The negative gate voltage on the left part of the nanochannel results in a negative effective surface charge, favoring the entry of  $\text{Rd}^+$  into the nanochannel. A similar phenomena of increasing the intensity of positively charged avidin on a negative gate voltage was observed by Karnik et al. (2006). However, the positive gate voltage on the right part of the nanochannel slows the movement of  $\text{Rd}^+$ , causing sample stacking in the nanochannel. The preconcentration effect is shown in Fig. 6a–e. Figure 6 clearly shows that  $\text{Rd}^+$  concentration becomes higher and higher in the nanochannel. This example demonstrates that the electrode-gated nanochannel can sample and preconcentrate the species simultaneously by controlling the applied potentials.

## 5 Conclusions

In this article, we examined the effect of gate voltage on the space charge density, electroosmotic flow, and ion transport in the nanochannel. The space charge density can be controlled by varying the applied gate voltage. For a constant gate voltage, the space charge density along the nanochannel is not a constant, but varies linearly along the nanochannel. The gate voltage can tune the nanochannel into a *p*-type or *n*-type field effect transistor. Bi-polarity is observed in the nanochannel. The fluid flow in the nanochannel can be controlled by varying the gate voltage. The ionic currents increase with increase in the space charge density. Analytical expressions derived for the space charge density, fluid flow and the ionic current are in reasonable agreement with the numerical simulations. The studies indicate that gated nanochannels can be employed as nanofluidic diodes and preconcentration devices.

**Acknowledgments** This study was supported by NSF under Grants 0120978 (the Water CAMPWS Center at UIUC), 0328162 (the nano-CEMMS Center at UIUC), Grant nos. 0810294, 0852657, and 0915718.

## References

- Aluru NR (2000) A point collocation method based on reproducing kernel approximations. *Int J Num Methods Eng* 47:1083–1121
- Aluru NR, Li G (2001) Finite cloud method: a true meshless technique based on a fixed reproducing kernel approximation. *Int J Num Methods Eng* 50:2373–2410
- Auroux PA, Iossifidis D, Reyes DR, Manz A (2002) Micro total analysis systems. 2 analytical standard operations and applications. *Anal Chem* 74:2637–2652
- Baldessari F, Santiago JG (2006) Electrophoresis in nanochannels: brief review and speculation. *J Nanobiotechnol* 4:12
- Belder D, Ludwig M (2003) Surface modification in microchip electrophoresis. *Electrophoresis* 24:3595–3606
- Chatterjee AN, Cannon DM, Gatimu EN, Sweedler JV, Aluru NR, Bohn PW (2005) Modeling and simulation of ionic currents in three-dimensional microfluidic devices with nanofluidic interconnects. *J Nanoparticle Res* 7:507–516
- Daiguji H, Oka Y, Shirono K (2005) Nanofluidic diode and bipolar transistor. *Nano Lett* 5:2274–2280
- Daiguji H, Yang P, Majumdar A (2004) Ion transport in nanofluidic channels. *Nano Lett* 4:137–142
- de Jong J, Lammertink RGH, Wessling M (2006) Membranes and microfluidics: a review. *Lab Chip* 6:1125–1139
- Eijkel JCT, van den Berg A (2005) What is it and what can we expect from it? *Microfluid Nanofluid* 1:249–267
- Fan R, Huh S, Yan R, Arnold J, Yang P (2008) Gated proton transport in aligned mesoporous silica films. *Nat Mater* 7:303–307
- Fan R, Yue M, Karnik R, Majumdar A, Yang P (2005) Polarity switching and transient responses in single nanotube nanofluidic transistors. *Phys Rev Lett* 95:086607
- Gatimu EN, Jin X, Aluru NR, Bohn PW (2008) Perturbation of microfluidic transport following electrokinetic injection through a nanocapillary array membrane: Injection and biphasic recovery. *J Phys Chem C* 112:19242–19247
- Gatimu EN, Sweedler JV, Bohn PW (2006) Nanofluidics and the role of nanocapillary array membranes in mass-limited chemical analysis. *Analyst* 131:705–709
- Hong JW, Quake SR (2003) Integrated nanoliter systems. *Nat Biotechnol* 21:1179–1183
- Horiuchi K, Dutta P (2006) Electrokinetic flow control in microfluidic chips using a field-effect transistor. *Lab Chip* 6:714–723
- Horvath J, Dolnik V (2001) Polymer wall coatings for capillary electrophoresis. *Electrophoresis* 21:644–655
- Jackson JD (ed) (1999) Classical electrodynamics, 3rd edn. Wiley, New York
- Jeon S, Malyarchuk V, White JO, Rogers JA (2005) Optically fabricated three dimensional nanofluidic mixers for microfluidic devices. *Nano Lett* 5:1351–1356
- Jin X, Joseph S, Gatimu EN, Bohn PW, Aluru NR (2007) Induced electrokinetic transport in micro-nanofluidic interconnect devices. *Langmuir* 23:13209–13222
- Jin X, Li G, Aluru NR (2001) On the equivalence between least-squares and kernel approximations in meshless methods. *Comput Model Eng Sci* 2:447–462
- Jin X, Li G, Aluru NR (2004) Positivity conditions in meshless collocation methods. *Comput Model Eng Sci* 193:1171–1202
- Jin X, Li G, Aluru NR (2005) New approximations and collocation schemes in the finite cloud method. *Comput Struct* 83:1366–1385
- Kalman EB, Vlassioux I, Siwy Z (2008) Nanofluidic bipolar transistors. *Adv Mater* 20:293–297
- Karniadakis GE, Beskok A, Aluru NR (eds) (2005) Microflows and Nanoflows: fundamentals and Simulation. Springer, New York
- Karnik R, Castelino K, Majumdar A (2006) Field-effect control of protein transport in a nanofluidic transistor circuit. *Appl Phys Lett* 88:123114
- Karnik R, Duan C, Castelino K, Daiguji H, Majumdar A (2007) Rectification of ionic current in a nanofluidic diode. *Nano Lett* 7:547–551
- Kuo TC, Cannon DM, Chen Y, Tulock JJ, Shannon MA, Sweedler JV, Bohn PW (2003a) Gateable nanofluidic interconnects for multilayered microfluidic separation systems. *Anal Chem* 75:1861–1867
- Kuo TC, Cannon DM, Shannon MA, Bohn PW, Sweedler JV (2003b) Hybrid three-dimensional nanofluidic/microfluidic devices using molecular gates. *Sens Actuators* 102:223–233
- Kuo TC, Kim HK, Cannon DM, Shannon MA, Sweedler JV, Bohn PW (2004) Nanocapillary arrays effect mixing and reaction in multilayer fluidic structures. *Angew Chem Int Ed* 43:1862–1865
- Lin JL, Lee K, Lee G (2006) Active micro-mixers utilizing a gradient zeta potential induced by inclined buried shielding electrodes. *J Micromech Microeng* 16:757–768
- Long TM, Prakash S, Shannon MA, Moore JS (2006) Water-vapor plasma-based surface activation for trichlorosilane modification of pmma. *Langmuir* 22:4104–4109
- Moghaddam S, Pengwang E, Jiang Y, Garcia AR, Burnett DJ, Brinker CJ, Masel RI, Shannon MA (2010) An inorganic-organic proton exchange membrane for fuel cells with a controlled nanoscale pore structure. *Nat Nanotechnol* 5:230–236
- Pennathur S, Santiago JG (2005) Electrokinetic transport in nanochannels 1 theory. *Anal Chem* 77:6772–6781
- Prakash S, Karacor M, Banerjee S (2009) Surface modification in microsystems and nanosystems. *Surf Sci Rep* 64:233–254
- Prakash S, Long TM, Selby JS, Moore JS, Shannon MA (2007) “click” modification of silica surfaces and glass microfluidic channels. *Anal Chem* 79:1661–1667
- Pu Q, Yun J, Temkin H, Liu S (2004) Ion-enrichment and ion-depletion effect of nanochannel structures. *Nano Lett* 4:1099–1103
- Reyes DR, Iossifidis D, Auroux PA, Manz A (2002) Micro total analysis systems. 1. Introduction, theory, and technology. *Anal Chem* 74:2623–2636
- Schasfoort RBM, Schlautmann S, Hendrikse L, van den Berg A (1999) Field-effect flow control for microfabricated fluidic networks. *Science* 286:942–945
- Schoch RB, Lintel HV, Renaud P (2005) Effect of the surface charge on ion transport through nanoslits. *Phys Fluids* 17:100604
- Schoch RB, Renaud P (2005) Ion transport through nanoslits dominated by the effective surface charge. *Appl Phys Lett* 86:253111
- Stein D, Kruithof M, Dekker C (2004) Surface-charge-governed ion transport in nanofluidic channels. *Phys Rev Lett* 93:035901
- Tulock JJ, Shannon MA, Bohn PW, Sweedler JV (2004) Microfluidic separation and gateable fraction collection for mass-limited samples. *Anal Chem* 76:6419–6425
- Vermesh U, Choi JW, Vermesh O, Fan R, Nagaraj J, Heath JR (2009) Fast nonlinear ion transport via field-induced hydrodynamic slip in ub-20-nm hydrophilic nanofluidic transistors. *Nano Lett* 9:1315–1319
- Vlassioux I, Siwy Z (2007) Nanofluidic diode. *Nano Lett* 7:552–556

- Wang Y, Stevens AL, Han J (2005) Million-fold preconcentration of proteins and peptides by nanofluidic filter. *Anal Chem* 77:4293–4299
- Yao S, Myers AM, Posner JD, Rose KA, Santiago JG (2006) Electroosmotic pumps fabricated from porous silicon membranes. *J Microelectromech Sys* 15:717–728
- Yaroshchuk A, Zhukowa O, Ulbricht M, Ribitsch V (2005) Electrochemical and other transport properties of nanoporous track-etched membranes studied by the current switch-off technique. *Langmuir* 21:6872–6882